Molten Gallium as a Non-Reactive Solvent: Synthesis of the Silicides $RE_2Ni_{3+x}Si_{5-x}$ (RE = Sm, Gd and Tb)

Marina A. Zhuravleva and Mercouri G. Kanatzidis

Department of Chemistry, Michigan State University, East Lansing, MI, 48824

Reprint requests to Prof. Dr. M. G. Kanatzidis. E-mail: kanatzid@cem.msu.edu

Z. Naturforsch. **58b,** 649–657 (2003); received February 25, 2003

The use of molten Ga as a non-reactive solvent for the synthesis of intermetallic silicides was demonstrated on the family $RE_2Ni_{3+x}Si_{5-x}$ (*RE* = Sm, Gd and Tb). The structure of $Sm_2Ni_{3+x}Si_{5-x}$ was solved from single crystal X-ray data in the orthorhombic space group *Ibam*, $Z = 4$, cell parameters $a = 9.6396(12)$; $b = 11.3219(14)$; and $c = 5.6967(13)$ Å. The refinement based on the full-matrix least-squares on F_o^2 [$I > 2\sigma(I)$] converged to final residuals $R_1/wR_2 = 0.0206/0.0492$. The structure of $RE_2Ni_{3+x}Si_{5-x}$ is related to the $U_2Co_3Si_5$ structure type; however, discrepancies exist between the solution obtained for $RE_2Ni_{3+x}Si_{5-x}$ and that reported for $U_2Co_3Si_5$. The magnetic properties studied on $Tb_2Ni_{3+x}Si_{5-x}$ indicate an antiferromagnetic ordering of magnetic moments centered at Tb ions at 13 K, and Curie-Weiss behavior at high temperatures with the effective moment close to that of free Tb^{3+} ion.

Key words: Flux Synthesis, Magnetism, Mixed Occupancy, Intermetallics

Introduction

As in any solvent system acting as a reaction medium, the solvent may or may not be incorporated into the final product. This is also what happens with gallium metal. Interestingly, working with molten Ga as a solvent, we find quite extreme examples it serving both as a reactive solvent producing polygallides [1, 2], and as a non-reactive solvent yielding Ga-free products [3]. Because silicides are technologically [4] essential for their high stability towards oxidation, hardness [5, 6], refractory properties [7, 8], interesting electronic and magnetic properties, such as superconductivity [9, 10] and coexistence of magnetism and superconductivity [11], it is important to explore and further develop preparative techniques for these materials. One of the challenges in synthesis of silicides and germanides is their high refractivity, *i. e.* very high temperatures are required for reaction to occur. As a consequence, it is rather difficult to prepare complex silicide compounds, since the reaction outcome is normally drawn to its thermodynamic minimum that often includes only the most stable simple binary compounds. The synthetic approach adopted in this work involves liquid Ga and allows lower reaction temperatures due to enhanced diffusion caused by partial solubility of the reactants. Results on the use of molten Ga as a non-reactive solvent for synthesis of silicides and germanides are rare. One examples is the synthesis of $EuZn_2Si_2$ and $EuZn_2Ge_2$ [12] from mixed Ga/Zn fluxes. Another comes from our own investigations and concerns the family $RENiSi_3$ [3, 13]. Here we report the synthesis, crystal structure and magnetic properties of rare-earth nickel silicides of the general formula $RE_2Ni_{3+x}Si_{5-x}$, (*RE* = Sm, Gd and Tb) obtained from molten Ga solutions.

Experimental Section

Synthesis

Elemental *RE* (Sm, Gd, Tb), Ni and Si of typical purity 99.9% and higher (CERAC Inc.) were combined together with a large excess of Ga in the ratio *RE*:Ni:Si:Ga as 1:2:2:30 and placed in the alumina crucibles. The metals were handled in a dry box under nitrogen atmosphere. The crucibles were then sealed in a quartz ampoule under vacuum ($\sim 1 \cdot 10^{-4}$ Torr). The reaction conditions, under which the first members of the $RE_2Ni_{3+x}Si_{5-x}$ group of compounds were obtained, included quite short heat treatment. In these reactions the metal mixtures were heated to 1000 °C in 15 h, held at 1000 °C for 5 h, then slowly cooled to 600 °C in 16 h, followed by fast cooling to 50 °C in 5 h. In order to improve crystal size and quality, heating profiles with longer isothermal steps were used. In these reactions, metal mixtures were heated to 1000 °C in 15 h, cooled down to 850 °C in 5 h and

held at 850 °C for 3 to 10 days, then cooled to 200 °C in 36 h and, finally, to 50 °C in 2 h.

The crystalline product obtained in these reactions was isolated from the Ga flux using 1–2 M solution of iodine in dimethylformamide (DMF) over six hours at 60 °C followed by a similar treatment at room temperature for ~ 18 h. The product was finally rinsed with DMF, water, and dried with acetone and ether. Crystals of $RE_2Ni_{3+x}Si_{5-x}$ with characteristic bar-like habit and metallic luster were recovered. The yield from the shorter time reactions was ~ 90%. Additionally, a binary $Ni_3(Ga,Si)_2$ phase [14] was detected in minor quantities as a by-product. An image of a typical crystal of $Sm_2Ni_{3+x}Si_{5-x}$ grown under Ga flux conditions, taken on a scanning electron microscope (SEM) JEOL JSM-35C, is shown in Fig. 1.

X-ray powder diffraction and elemental analysis

The X-ray powder diffraction (XRD) patterns of products were taken at room temperature on a CPS 120 INEL X-ray diffractometer (Cu-K_α radiation) equipped with position-sensitive detector. Experimental XRD patterns were then compared to that calculated from single crystal data using the CERIUS^2 software package [15].

The elemental composition was studied by Energy Dispersive Spectroscopy (EDS) semi-quantitative analysis on the SEM equipped with the NORAN Inc. EDS detector. The data acquisition was normally done at an acceleration voltage of 20 kV and collection time 30 s. The results obtained on a large number of crystals were averaged in order to obtain more accurate values of the atomic ratios. For the Sm analog only RE, Ni and Si were detected. Although a small amount of Ga was occasionally observed in the EDS results (up to 5 at.%), it was later attributed to surface impurities from incompletely removed flux. Analysis taken on a freshly exposed cross-section of the crystal showed an absence of Ga. However, for the Tb analog, the situation seems to be different, as the elemental analysis taken on both surface and the cross-section showed a substantial amount of Ga present. The composition of the Tb analog could be formulated as "$Tb_2Ni_{2.77}Si_{4.63}Ga_{0.64}$".

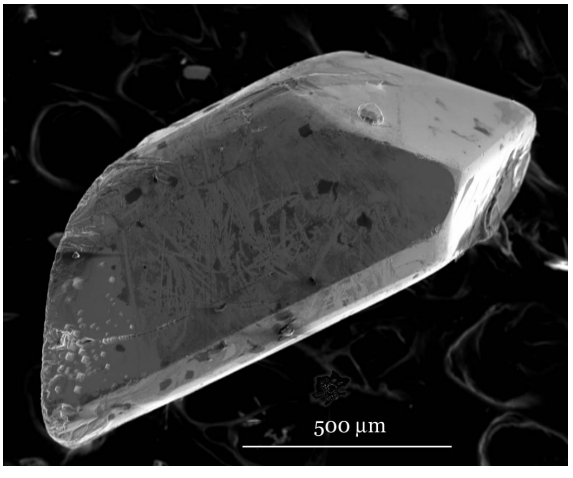

Fig. 1. SEM image of a typical Ga flux-grown single crystal of $Sm_2Ni_{3+x}Si_{5-x}$. The surface roughening is caused by an etching process during isolation.

Single crystal X-ray diffraction

The intensity data was collected on a single crystal of $Sm_2Ni_{3+x}Si_{5-x}$ at 173 K with a Siemens Platform SMART [16] CCD X-ray diffractometer. A crystal of suitable size (Table 1) was mounted on

Table 1. Crystal data and structure refinement for $Sm_2Ni_{3+x}Si_{5-x}$.

Empirical formula	$Sm_2Ni_{3+x}Si_{5-x}$
x	0.47(1)
Formula weight	631.98
Temperature [K]	173(2)
Wavelength [Å]	0.71073
Crystal system	orthorhombic
Space group	*Ibam* (# 72)
Unit cell dimensions [Å]	a = 9.6396(12) b = 11.3219(14) c = 5.6967(7)
Volume [Å^3]	621.73(13)
Z	4
Density (calculated) [g/cm^3]	6.752
Absorption coefficient [mm^{-1}]	29.662
F(000)	1139
Crystal size [mm^3]	0.04 × 0.06 × 0.12
θ Range for data collection	2.78 to 27.88°
Index ranges	$-12 \le h \le 10$, $-14 \le k \le 9$, $-7 \le l \le 7$
Reflections collected	1867
Independent reflections	411 [R_{int} = 0.0306]
Completeness to θ = 27.88°	99.8%
Refinement method	Full-matrix least-squares on F2
Data/restraints/parameters	411/0/33
Goodness-of-fit on $F2$	1.001
Final R indices [$I > 2\sigma(I)$]	R_1 = 0.0206, wR_2 = 0.0492
R indices (all data)	R_1 = 0.0252, wR_2 = 0.0510
Extinction coefficient	0.00080(10)
Largest diff. peak and hole [e·Å^{-3}]	1.149 and −0.928

$R_1 = \Sigma||F_o| - |F_c||/\Sigma|F_o|$; $wR_2 = [\Sigma w\{|F_o| - |F_c|\}^2/\Sigma w|F_o|^2]^{1/2}$.

glass fiber. A hemisphere of reciprocal data (Mo-K_α radiation, λ = 0.71073 Å) was acquired. The individual frames were measured using the ω-steps of 0.30° and an exposure time of 30 s per frame. The data reduction and integration was performed with the SAINTPLUS software package. An empirical correction for absorption based on symmetry equivalent reflections was applied with the SADABS program. The structure solution and refinement were done by direct methods with the SHELXTL software package. All atomic positions were refined anisotropically. The setting of the cell was standardized with the STRUCTURE TIDY program [17]. The information relevant to the data collection and structure refinement is given in the Table 1. The final atomic positions and the equivalent atomic displacement parameters are listed in Table 2. The interatomic distances up to 3.5 Å and selected bond angles are presented in Tables 3 and 4, respectively. The cif file for $Sm_2Ni_{3+x}Si_{5-x}$ has been deposited with ICSD-Fachinformationszentrum Karlsruhe, CSD 413051, e-mail: crysdat@fiz-karlsruhe.de

The crystal structure of $Sm_2Ni_{3+x}Si_{5-x}$ is related to the previously reported $U_2Co_3Si_5$ structure type [18a]. However, the refined structure of $Sm_2Ni_{3+x}Si_{5-x}$ based on single crystal X-ray diffraction data revealed severe discrepancies with that reported for $U_2Co_3Si_5$. The problem is the assignment of the atomic positions of the transition metal (Co or Ni) and Si in these two structures. In $U_2Co_3Si_5$, out of six atomic sites two (*4a* and *8j*) were assigned to Co atoms, three (*4b*, *8g*, *8j*) to Si atoms, and one site *8j* to U. Similarly, during the structure refinement of $Sm_2Ni_{3+x}Si_{5-x}$, a total of six atomic sites were identified. However, our refinement showed that the Ni atoms were located at the *4b* and *8j* sites, while the Si atoms were found at three sites with multiplicities *4a*, *8g* and *8j*. The Sm atoms were also found at the *8j* site. These results are consistent with the refinement given for the $Y_2Ni_3Si_5$ [18b]. Moreover, further structural refinement revealed an appreciable population of the Si *8j* site with Ni. The introduction of the Si/Ni mixed occupancy site at *8j* led to substantial reduction in *R*-values from 0.043 to 0.021 in the consecutive refinement cycle. The occupancy parameters of 0.763(7) and 0.237(7) were determined for Si and Ni at *8j*, respectively. The resulting convergence factor 0.0206 [for 368 reflections with $I > 2\sigma(I)$] [19] undoubtedly demonstrates the correctness of the atomic assignment presented herein. The exact empirical formula is $Sm_2Ni_{3+x}Si_{5-x}$ ($x = 0.237(7)$, $Z = 4$). Given the high level of the structure refinement achieved for $Sm_2Ni_{3+x}Si_{5-x}$ we are led to question the accuracy of the reported structure of $U_2Co_3Si_5$ and to suggest that it be re-examined.

Magnetic measurements

The magnetic susceptibility was measured on polycrystalline samples of $Tb_2Ni_{3+x}Si_{5-x}$ as a func-

Table 2. Atomic coordinates, equivalent isotropic displacement parameters (Å$^2 \times 10^3$) and occupancies for $Sm_2Ni_{3+x}Si_{5-x}$.

Atomic Position	Wyckoff Symbol	*x*	*y*	*z*	U(eq)*	Occupancy
Sm	*8j*	0.2626(1)	0.3692(1)	0	4(1)	1.0
Ni(1)	*4b*	1/2	0	1/4	6(1)	1.0
Ni(2)	*8j*	0.1124(1)	0.1323(1)	0	6(1)	1.0
Si(1)	*4a*	0	0	1/4	3(1)	1.0
Si(2)	*8j*	0.3491(2)	0.1069(2)	0	4(1)	1.0
Si/Ni	*8g*	0	0.2654(1)	1/4	4(1)	0.763(7) Si+ 0.237(7) Ni

*U(eq) is defined as one third of the trace of the orthogonalized U_{ij} tensor.

Table 3. Bond lengths [Å] for $Sm_2Ni_{3+x}Si_{5-x}$.

Bond	Distance	Mult.	Bond	Distance	Mult.
Sm – Ni(1)	3.2599(4)	×2	Sm – Si/Ni	3.1331(7)	
Sm – Ni(2)	3.0481(9)		Ni(1) – Si(2)	2.3685(14)	×4
Sm – Ni(2)	3.2128(10)		Ni(1) – Si/Ni	2.6562(15)	×2
Sm – Ni(2)	3.3726(11)		Ni(1) – Ni(1)	2.8484(4)	×2
Sm – Ni(2)	3.0927(5)	×2	Ni(2) – Si(2)	2.299(2)	
Sm – Si(1)	3.0755(4)	×2	Ni(2) – Si(1)	2.3336(7)	×2
Sm – Si(2)	3.0568(7)	×2	Ni(2) – Si/Ni	2.3398(12)	×2
Sm – Si(2)	2.898(2)		Si(1) – Si(1)	2.8484(4)	×2
Sm – Si(2)	3.0849(19)		Si(2) – Si/Ni	2.4973(17)	×2
Sm – Si/Ni	3.0966(8)	×3	Si/Ni – Si/Ni	2.8483(4)	×2

Table 4. Selected bond angles [°] for $Sm_2Ni_{3+x}Si_{5-x}$.

Bond	Angle	Bond	Angle
Si(2)–Ni(1)–Si(2)	106.07(5)	Ni(2)–Si(2)–Ni(1)	132.33(6)
Si(2)–Ni(1)–Si(2)	104.19(8)	Ni(1)–Si(2)–Ni(1)	73.93(5)
Si(2)–Ni(1)–Si(2)	118.55(9)	Ni(1)–Si(2)–Si/Ni	66.11(5)
Si(2)–Ni(1)–Si/Ni	59.28(4)	Si/Ni–Si(2)–Si/Ni	69.54(6)
Si/Ni–Ni(1)–Si/Ni	180.0	Ni(2)–Si(2)–Si/Ni	120.37(7)
Si(2)–Ni(1)–Si/Ni	120.72(4)	Ni(1)–Si(2)–Si/Ni	106.31(7)
Si(2)–Ni(1)–Ni(1)	126.96(3)	Ni(1)–Si(2)–Ni(1)	73.93(5)
Si(2)–Ni(1)–Ni(1)	53.04(3)	Ni(2)–Si/Ni–Ni(1)	130.10(3)
Si/Ni–Ni(1)–Ni(1)	90.0	Si(2)–Si/Ni–Ni(1)	54.62(5)
Ni(1)–Ni(1)–Ni(1)	180.0	Ni(2)–Si/Ni–Si/Ni	127.49(2)
Si(1)–Ni(2)–Si(1)	75.22(3)	Si(2)–Si/Ni–Si/Ni	55.23(3)
Si(1)–Ni(2)–Si/Ni	80.02(3)	Ni(1)–Si/Ni–Si/Ni	90.0
Si(1)–Ni(2)–Si/Ni	124.73(4)	Ni(2)–Si/Ni–Si/Ni	52.51(2)
Si(2)–Ni(2)–Si/Ni	122.69(4)	Si(2)–Si/Ni–Si/Ni	124.77(3)
Si/Ni–Ni(2)–Si/Ni	74.99(4)	Si/Ni–Si/Ni–Si/Ni	180.0
Si(2)–Ni(2)–Si(1)	112.37(5)	Ni(2)–Si/Ni–Si(2)	107.21(3)
Ni(2)–Si(1)–Ni(2)	104.78(3)	Si(2)–Si/Ni–Si(2)	109.23(9)
Ni(2)–Si(1)–Ni(2)	100.15(4)	Ni(2)–Si/Ni–Ni(2)	99.79(6)
Ni(2)–Si(1)–Ni(2)	124.65(4)	Ni(2)–Si/Ni–Si(2)	116.76(4)

tion of temperature in the range 2–400 K in an applied external magnetic field of 500 G with MPMS Quantum Design Inc. SQUID magnetometer. The susceptibility data was corrected for the sample holder contribution.

Results and Discussion

Reaction chemistry

A number of isotypes [20] of the $U_2Co_3Si_5$ family of compounds have been reported in the literature including $RE_2Ni_3Si_5$ [21,22]. The generalized formula could be represented as $A_2M_3Tt_5$, where A can be actinide or lanthanide, M is a transition metal (*3d*, *4d* and *5d*) and Tt is a tetrel element (Si, Ge and Sn). The above mentioned compounds were obtained in small crystalline or polycrystalline form from arc-melting reactions with subsequent annealing. In contrast, large single crystals (up to few millimeters on the side) of the $RE_2Ni_{3+x}Si_{5-x}$ (*RE* = Sm, Gd and Tb) family of compounds could be easily grown from molten Ga solutions at 850 °C. Although the highest yield of this phase was obtained from reactions with a short isothermal step, the crystal size noticeably improved upon prolonged heating of the reaction mixture. Thus, large well-faceted crystals were isolated from the reactions with 3 and 10 days for the isothermal step, Fig. 1. Additionally, the amount of Ga flux seems to play a role in the formation of the Ga-free $RE_2Ni_{3+x}Si_{5-x}$ phase. For example, from four sets of experiments using 8, 16, 30 and 40 equivalents of Ga, under otherwise identical conditions, the ternary silicides ($RE_2Ni_{3+x}Si_{5-x}$ and $RENiSi_3$) preferably form at the extreme ends with a Ga content of 8 or 40. The medium Ga content (16 or 30) instead promotes formation of the quaternary $RE_{0.67}Ni_2Ga_{5+n-x}Si_x$ (n = 0,1) phases [23].

Interestingly, the Ge analog of the $RE_2Ni_{3+x}Si_{5-x}$ phase could not be obtained from similar reactions with Ge. In germanium containing reactions Ga invariably gets incorporated in the final product, giving rise to quaternary phases like $RE_{0.67}M_2Ga_{5+n-x}Ge_x$ [23] (n = 0,1), $RE_2MGa_9Ge_2$ [24], $RE_4Ni_3Ga_6Ge_4$ [24], $REMGa_3Ge$ [25] and $RE_3Ni_3Ga_8Ge_3$ [25], where M = Ni or Co. Similarly, molten Al solutions could not be used for the synthesis of transition metal silicides such as $RE_2Ni_{3+x}Si_{5-x}$ or $RENiSi_3$ [3], as Al always integrates into the product. The capability of molten Ga to serve as a non-reactive solvent under certain conditions to form silicides is thus of great interest.

Crystal structure

The drawing of the crystal structure of $Sm_2Ni_{3+x}Si_{5-x}$ projected onto the *ab*-plane is depicted in Fig. 2A. For simplicity, the bonds to Sm atoms were omitted. The structure is three-dimensional (3D), although for a better understanding it is worthwhile to sub-divide it into a pair of slabs. The first one is a two-dimensional $\{Ni_{3+x}Si_{5-x}\}$

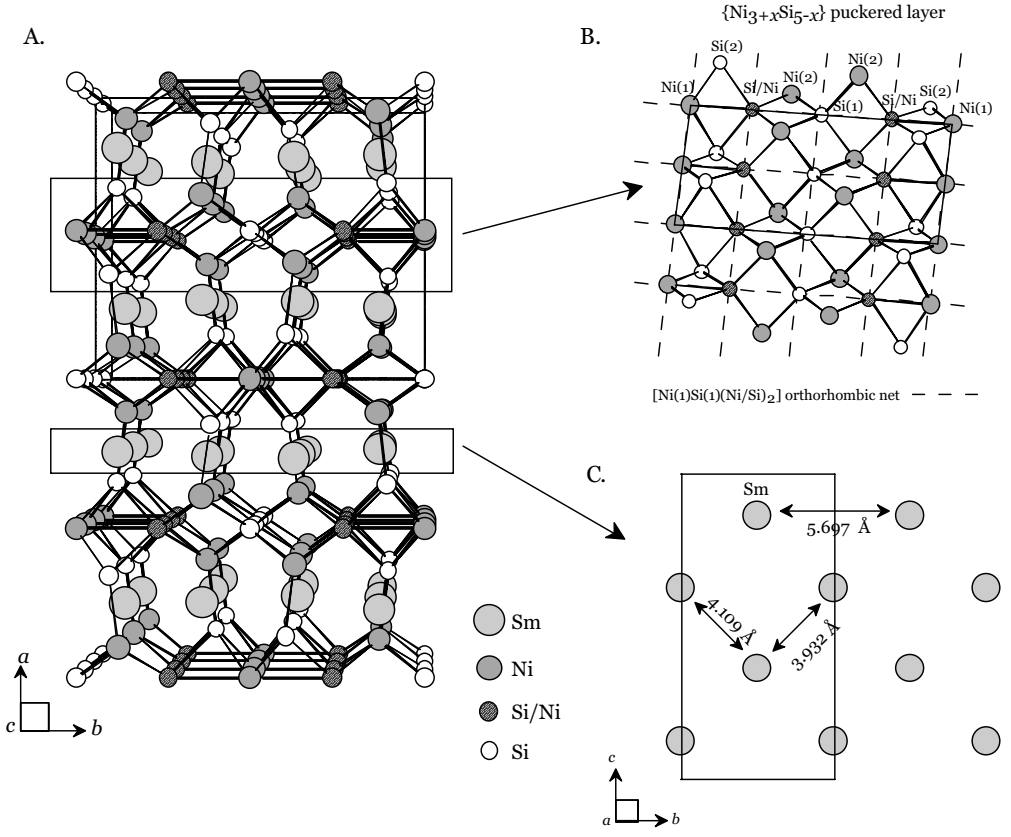

Fig. (A) The structure of $Sm_2Ni_{3+x}Si_{5-x}$ viewed along the *c*-axis. The unit cell is drawn in bold line; (B) $\{Ni_{3+x}Si_{5-x}\}$ puckered layer viewed approximately along the *a*-axis. The unit cell is indicated with bold line. A distorted square net is outlined in dashed lines; (C) The Sm-only structural fragment projected onto the *bc*-plane. The closest bonding contacts are indicated by the arrows and the distance is given in Å.

puckered layer, shown in Fig. 2B. In this layer, the Ni(1) and Si(1) atoms form a distorted square net, which is outlined by the dashed contour. The atoms of Ni(2) and Si(2) are situated alternating above and below the squares.

In the intermetallic compounds containing a *RE*, a transition metal (M) and a tetrel element (Tt), the occurrence of the puckered layers (reminiscent of the PbO structure) consisting of square nets of M atoms capped with Tt element (denoted "MTt" for brevity) and vice versa (TtM) are widespread. For instance, the representatives of the $ThCr_2Si_2$ structure type, such as exhibit a "MTt" arrangement, where the M atoms define the square net, and the Tt elements serve as capping atoms. The examples of the inverse "TtM" arrangement where the Tt element are in the square net with M-type atoms capping it are even more common [26,27,28]. The inverse "TtM" arrangement also exists in a number of quaternary compounds such as $REMGa_3Ge$ [25], $RE_3Ni_3Ga_8Ge_3$ [25] and $RE_4Ni_3Ga_6Ge_4$ [24]. The mixing of M with Tt on the capping site of the "TtM" net is known as well ($Ce_3Ni_2Si_8$ [29]). However, the M/Tt arrangement in the puckered $\{Ni_{3+x}Si_{5-x}\}$ layer is unique in one sense. In the corners of the $\{Ni_{3+x}Si_{5-x}\}$ distorted square both Si(1), Ni(1) as well as mixed Si/Ni atomic sites are present. Likewise, the capping elements are both Si and Ni (atomic sites Si(2) and Ni(2)). Thus, in $Sm_2Ni_{3+x}Si_{5-x}$, the Ni and Si elements are distributed nearly evenly throughout the puckered layer (the equal Si and Ni content would occur for $x = 1$). This particular feature differentiates

$Sm_2Ni_{3+x}Si_{5-x}$ from all other compounds where a M/Tt puckered layer is observed. Because the electronic properties and bonding interactions of such networks are of continuing interest [30, 31, 32], discovery of another slightly different type of M/Tt net is valuable for future studies aimed at a better understanding of the electronic properties, origin of stability and the nature of chemical bonding in intermetallic compounds.

The second type of slab in $Sm_2Ni_{3+x}Si_{5-x}$ is a distorted square net of Sm atoms. This Sm-only monoatomic layer viewed down the *a*-axis is shown in Fig. 2C. The Sm-only plane and the $\{Ni_{3+x}Si_{5-x}\}$ puckered layer alternate along the *a*-axis to build the 3D structure.

The local coordination environments of the Ni and Si atoms within 3.0 Å and Sm atoms within 3.5 Å are presented in Fig. 3. The Ni(1) atoms have a total of eight Si and Ni atoms in their immediate coordination environment. Four Si(2) atoms are bonded at 2.3685(14) Å to Ni(1) in the form of a distorted tetrahedron. The Si(2)–Ni(1)–Si(2) angles deviate slightly from the ideal tetrahedral (104.19(8)°, 106.07(5)° and 118.55(9)°). The remaining four atoms of the Ni(1) coordination sphere are two Si/Ni (Ni(1)–Ni/Si = 2.6562(15) Å) and two Ni(1) atoms (Ni(1)–Ni(1) = 2.8484(4) Å), arranged in-plane with a central Ni(1) atom. The Ni(2) atoms are in a distorted square pyramidal environment of Si and Ni atoms. The square base of the pyramid consists of two Si(1) atoms (Ni(2)–Si(1) = 2.3336(7) Å) and two Si/Ni atoms (Ni(2)–Si/Ni = 2.3398(12) Å). The apex of the pyramid is a Si(2) atom, at 2.299(2) Å from Ni(2). This is the shortest bond distance found in the structure.

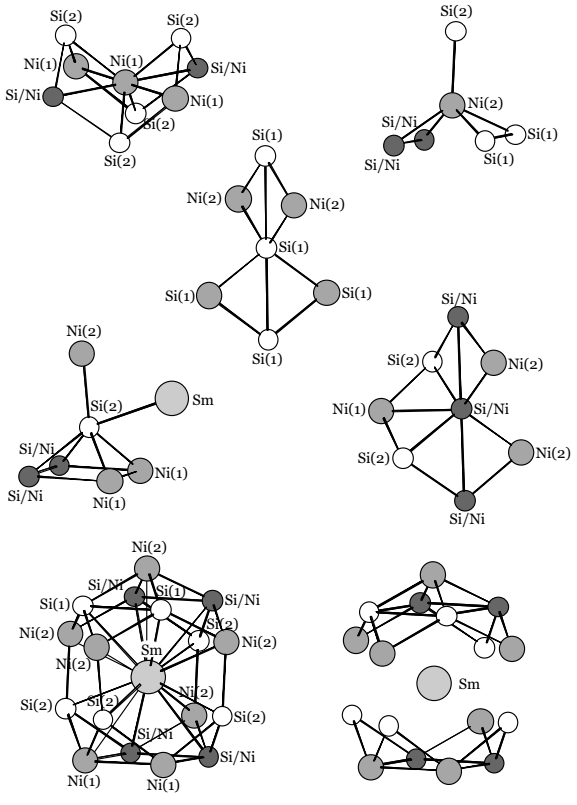

Fig. 3. Local coordination environment of the Sm atoms within the sphere of radius 3.5 Å, and Ni and Si atoms within 3.0 Å.

The Si(1) atoms are six-coordinate, and they are bonded to four Ni(2) atoms in the shape of a slightly distorted tetrahedron (Ni(2)–Si(1)–Ni(2) angles are 100.15(4)°, 124.65(4)° and 104.78(3)°). Two additional Si(1) atoms cap the edges of the tetrahedron and are located in line at 2.8484(4) Å from the central Si(1) atom. The Si(2) atoms have a mono-capped distorted square pyramidal environment. The pyramid is built up from a base consisting of two Si/Ni atoms and two Ni(1) atoms, with an apex of a Ni(2) atom. The capping Sm atom is located at 2.898(2) Å from Si(2), see Fig. 3.

The Sm atoms are 17-coordinate, bonded within 3.5 Å to four Si(2) atoms, five Ni(2) atoms, two Si(1) atoms, four Si/Ni atoms and two Ni(1) atoms. The coordination polyhedron of the Sm atom is rather complex, see Fig. 3. In the pictorial representation displayed on the right, no bonds were drawn to the central Sm atom, as well as between Ni(2) and Si(2) atoms. In this view, the Sm atom is positioned in a crib of eight Si and Ni atoms (below) and capped with another nine Si and Ni atoms (above).

Crystal chemistry and chemical bonding

It is rather difficult to judge the electron charge distribution in $RE_2Ni_{3+x}Si_{5-x}$, and intermetallic compounds in general, save for simple electronegativity considerations that may be applied. The situation may be somewhat simplified if we assume that the *RE* atoms which are the least electronegative are tri-positive, as indicated by the magnetic data (see below). Thus, a formal charge could be assigned to the whole $\{Ni_{3+x}Si_{5-x}\}$ framework, giv-

ing $\{Sm_2\}^{6+}\{Ni_{3+x}Si_{5-x}\}^{6-}$. For a more quantitative assessment of charge on the Ni and Si atoms, electronic structure calculations ought to be performed.

On the basis of connectivity arguments, it follows that the strongest bonding interaction takes place between adjacent $\{Ni_{3+x}Si_{5-x}\}$ slabs, which are linked *via* Ni(2)–Si(2) bonds at 2.299(2) Å. This is similar to the situation in $RENiSi_3$ [3], where the closest bonding contacts also occur between Ni and Si with an average Ni–Si distance of 2.293 Å (*RE* = Sm). For $RENiSi_3$, the theoretical electronic band structure calculations suggested that the Ni atoms have completely filled and greatly stabilized d-orbitals and thus are the most "reduced" species in the structure. By extension, it is plausible to assume that a similar situation may also hold true for $RE_2Ni_{3+x}Si_{5-x}$, given that the magnetic data (to be presented below) also do not reveal any measurable moment on the Ni atoms. This "reduction" gives rise to an electron-rich configuration of the Ni atoms ($3d^{10}$ or $4s^23d^{10}$), and is most likely to explain the relatively short bonding contacts between Ni–Si and Ni–Sm atoms and the non-magnetic behavior of the Ni atoms.

The bonding within the $\{Ni_{3+x}Si_{5-x}\}$ layer and between the Sm and $\{Ni_{3+x}Si_{5-x}\}$ slabs is also strong. Thus, the Si–Ni and Si–Si distances cover the range of 2.3336(7)–2.6561(15) Å and 2.4973(17)–2.8483(4) Å, respectively. The average Ni–Si and Si–Si bond distances found in $Sm_2Ni_{3+x}Si_{5-x}$ are respectively 2.402 and 2.673 Å, and are comparable to the sum of the single-bonded metallic radii [33] of Ni and Si (2.39 and 2.36 Å). Similar Si–Ni distances of 2.283(2), 2.295(3) and 2.303(1) Å were also found in the related $SmNiSi_3$ compound [3]. The contacts between the Sm and Ni and Si atoms are likewise bonding, with Sm–Ni and Sm–Si bond lengths of 3.191 and 3.067 Å on average, respectively. In contrast, the Sm–Sm distances in the Sm distorted square plane are 3.932 and 4.109 Å, and they are considered non bonding.

The Si/Ni mixed occupancy site at *8j* is responsible for the slight deviation from the ideal stoichiometry of $RE_2Ni_3Si_5$. The analogous compounds reported in the literature have not been structurally characterized at the same level of detail reported here. We surmise that these too are in fact non-stoichiometric in the manner found for the flux grown $Sm_2Ni_{3+x}Si_{5-x}$.

Magnetic properties

The magnetism of the $Tb_2Ni_{3+x}Si_{5-x}$ analog was studied as a function of temperature. The magnetic susceptibility goes through a maximum at ~ 13 K characteristic of an antiferromagnetic ordering. The Néel temperature of an antiferromagnetic transition T_N = 13.2 K was deduced from a set of isofield χ_m-T measurements. Above 30 K, the reciprocal magnetic susceptibility increases linearly with temperature, following the Curie-Weiss law. The effective magnetic moment and the Weiss constant, obtained from the linear part of the temperature dependence of the inverse magnetic susceptibility, are 9.69 μ_B and −8.4 K, respectively. The experimental value of the effective magnetic moment agrees well with the theoretical value [34] (9.72 μ_B) for the Tb^{3+} ion. These results agree well with earlier studies reported for $Tb_2Ni_3Si_5$. A neutron derived magnetic structure for $Tb_2Ni_3Si_5$ was also determned [35, 36].

The magnetism in $RE_2Ni_{3+x}Si_{5-x}$ is caused solely by the magnetic moments localized on the RE ions, whilst Ni atoms are in a non-magnetic state. A similar situation was observed in a number of intermetallic compounds containing both RE and Ni as possible magnetic centers [37, 38, 3, 23, 25].

Concluding Remarks

Large single crystals of $RE_2Ni_{3+x}Si_{5-x}$ (*RE* = Sm, Gd and Tb) adopt the $U_2Co_3Si_5$-structure type and could be easily grown from solutions of molten Ga at relatively moderate temperatures (850 °C). The X-ray structure solution of $Sm_2Ni_{3+x}Si_{5-x}$ revealed the following atomic positions: *4b* and *8j* for Ni atoms, *4a*, *8 g*, *8j* for Si atoms, and *8j* site for RE atom. The *8j* site was found to contain both Si and Ni. These results cast doubt on the correctness of the reported structure of $U_2Co_3Si_5$ and calls for a reinvestigation. The structure is built by consecutive stacking of orthorhombic $\{Sm_2\}$ monoatomic planes and $\{Ni_{3+x}Si_{5-x}\}$ puckered layers. The peculiar characteristic of the $\{Ni_{3+x}Si_{5-x}\}$ puckered layer is the absence of a distinct separation into the Si square net capped with Ni atoms (or *vice versa*). Instead, both Si and Ni are uniformly participating in constructing the

square lattice and capping elements. This is in contrast to what has so far been observed in a large number of intermetallic silicides. Recent magnetoresistance (MR) studies on polycrystalline $RE_2Ni_3Si_5$, (R = Nd, Sm, Tb), which order antiferromagnetically at low temperatures, showed positive giant magnetoresistance [39]. The availability of single crystals of these materials should help to study this phenomenon at a deeper level.

Acknowledgements:

Financial support from the Department of Energy (Grant # DE-FG02-99ER45793) is gratefully acknowledged. This work made use of the SEM/EDS facilities of the Center of Advanced Microscopy at Michigan State University.

[1] X. Z. Chen, P. Small, S. Sportouch, M. Zhuravleva, P. Brazis, C. R. Kannewurf, and M. G. Kanatzidis, Chem. Mater., **12**, 2520 (2000).
[2] M. A. Zhuravleva and M. G. Kanatzidis, J. Solid State Chem. (2003), in press.
[3] X. Z. Chen, P. Larson, S. Sportouch, P. Brazis, S. D. Mahanti, C. R. Kannewurf, and M. G. Kanatzidis, Chem. Mater. **11**, 75 (1999).
[4] C. Witham, B. V. Ratnakumar, R. C. Bowman (Jr.), A. Hightower, B. Fultz, J. Electrochem. Soc. **143**, L205, (1996).
[5] K. S. Kumar, in J. H. Westbrook and R. L. Fleischer (eds): Intermetallic Compounds, Principles and Practice, Vol. 2, Chapter 10, p. 221, Wiley, New York (1995).
[6] A. K. Vasudévan and J. J. Petrovic, Materials Science and Engineering A – Structural Materials, Properties, Microstructure and Processing **155**, 1 (1992).
[7] D. M. Shah, D. Berczik, D. L. Anton, and R. Hecht, Materials Science and Engineering A – Structural Materials, Properties, Microstructure and Processing **155**, 45(1992).
[8] (a) P. J. Meschter and D. S. Schwartz, J. Metals, **41**, 52 (1989); (b) H. Inui, M. Moriwaki, K. Ito, and M. Yamaguchi, Phil. Mag. **77**, 375 (1998).
[9] B. Chevalier, P. Lejay, J. Etourneau, and P. Hagenmuller, Mater. Res. Bull. **8**, 315 (1983).
[10] a) H. F. Braun, J. Less-Common Met. **100**, 105 (1984); b) X.-Z. Wang, B. Lloret, W. L. Ng, and B. Chevalier, J. Etourneau, P. Hagenmuller, Revue de Chemie Minér. **22**, 711 (1985).
[11] H. Nakamura, Y. Kitaoka, H. Yamada, and K. Asayama, J. Magn. Magn. Mater. **76&77**, 517(1988).
[12] A. Grytsiv, D. Kaczorowski, A. Leithe-Jasper, P. Rogl, C. Godart, M. Potel, and H. Noël, J. Solid State Chem. **163**, 37 (2002).
[13] J. Salvador and M. G. Kanatzidis, work in progress.
[14] $Ni_3Ga_{2-x}Si_x$ pseudo binary phase grows readily form Ga flux as thin plates. Single crystal X-ray data: P-3 m1, a = 4.006(2) Å, c = 4.874(2) Å, R_1/wR_2 = 0.0487/0.0491 for $I > 2\sigma(I)$, residual peak/hole +1.746/–2.853. Despite the fact that Si was found in appreciable amounts in EDS elemental analysis (formula "$Ni_8Ga_9Si_3$"), no Si could be located during structural refinement. Two Ni positions at 1b and 2d and single Ga site at 2d were refined.
[15] CERIUS^2, Version 1.6 Molecular Simulations Inc., Cambridge, England (1994).
[16] a) SMART, Version 5; Siemens Analytical X-ray Systems, Inc., Madison, WI (1998); b) SAINT, Version 4; Siemens Analytical X-ray Systems, Inc., Madison, WI (1994–96).
[17] L. M. Gelato and E. Parthé, J. Appl. Crystallogr. **20**, 139 (1987).
[18] a) L. G. Aksel'rud, Ya. P. Yarmolyuk, and E. I. Gladyshevskii, Sov. Phys. Crystallogr. **22**, 492 (1977); b) B. Chabot, E. Parthé, J. Less-Common Met. **97**, 285 (1984).
[19] Compare to R-value of 0.122 reported for $U_2Co_3Si_5$.
[20] P. Villars and L. D. Calvert, Pearson's Handbook of Crystallographic Data for Intermetallic Phases, ASM International, Materials Park, OH (1991).
[21] Y. K. Gorelenko, R. V. Skolozdra, I. D. Shcherba, and V. I. Yarovets, Inorg. Mater. **29**, 1471 (1993).
[22] O. I. Bodak, Y. K. Gorelenko, VI Yarovets, I. D. Shcherba, G. A. Mel'nik A, L. O. Dobryanskaya, and R. V. Skolozdra, Inorg. Mater. **35**, 360 (1999).
[23] M. A. Zhuravleva, X. Z. Chen, X. Wang, A. J. Schultz, J. Ireland, C. R. Kannewurf, and M. G. Kanatzidis, Chem. Mater. **14**, 3066 (2002).
[24] M. A. Zhuravleva, Ph.D. Dissertation, Michigan State University (2002).
[25] M. A. Zhuravleva, R. J. Pcionek, X. Wang, A. J. Schultz, and M. G. Kanatzidis, Inorg. Chem. (2003), in press.

[26] O. P. Bodak and E. I. Gladyshevskii, Soviet Physics-Crystallogr., translated from Kristallografiya **14**, 859 (1970).
[27] K. Cenzual, R. E. Gladyshevskii, and E. Parthé, Acta Crystallogr. Sec. C. **48**, 225 (1992).
[28] V. V. Pavlyuk, O. I. Bodak, and A. N. Sobolev, Sov. Phys. Crystallogr. **36**, 493 (1991).
[29] J. A. Stepien, K. Lukaszewicz, E. I. Gladyshevskii, and O. I. Bodak, Bull. Acad. Pol. Sci. Ser. Sci. Chim. **20**, 1029 (1972).
[30] a) C. Zheng and R. Hoffman, J. Am. Chem. Soc. **108**, 3078 (1986); b) R. Hoffman, C. Zheng, J. Phys. Chem. **89**, 4175 (1985); c) W. Tremel, R. Hoffman, J. Am. Chem. Soc. **109.** 124 (1987); d) G. Trinquier, R. Hoffman, J. Phys. Chem. **88**, 6696 (1984).
[31] D. M. Prosperio, G. Chacon, and C. Zheng, Chem. Mater. **10**, 1286 (1998).
[32] D. M. Prosperio, G. Artioli, S. Mulley, G. Chacon, and C. Zheng, Chem. Mater. **9**, 1463 (1997).
[33] G. Wulfsberg, in "Inorganic Chemistry", p. 32, University Science Books: Sausalito, California (2000).
[34] The theoretical value for effective magnetic moment is given by the formula $g_J \cdot [J(J+1)]^{1/2}$, where g_J is a Landé factor and J is a total angular momentum of the Tb^{3+} ion.
[35] S. Skanthakumar, J. W. Lynn, C. Mazumdar, R. Nagarajan, and L. C. Gupta, Physica B **241**, 693 (1997).
[36] A. Szytula, M. Kolenda, E. Ressouche, and W. Sikora, J. Phys.-Cond. Matter **9**, 6651 (1997).
[37] X. Z. Chen, S. Sportouch, P. Brazis, C. R. Kannewurf, J. A. Cowen, R. Patschke, and M. G. Kanatzidis, Chem. Mater. **10**, 3202 (1998).
[38] B. Sieve, X. Z. Chen, J. A. Cowen, P. Larson, S. D. Mahanti, and M. G. Kanatzidis, Chem. Mater. **11**, 2451 (1999).
[39] C. Mazumdar, A. K. Nigam, R. Nagarajan, L. C. Gupta, G. Chandra, B. D. Padalia, and C. Godart, R. Vijayaraghaven, J. Appl. Phys. **81**, 5781 (1997).